APPENDIX: DATA REPOSITORY BACKGROUND INFORMATION ON GEOMORPHOLOGY AND AGE CONTROL OF THE EKSIK STUDY SITE

I. Geomorphologic setting of the Eksik Study Site

The Eksik study site lies along the central part of the North Anatolian fault (Fig. DR1). This reach of the fault ruptured most recently during the 1943 M_w 7.7 Tosya earthquake. The surface trace in the Eksik area is generally linear, as can be seen in figures DR2 and DR3. Figure DR4 shows a general view of the study site looking towards the south-southwest, with the fault extending across the site as a narrow, well-defined, west-southwest-trending zone. The offset fluvial terrace that forms the basis for our slip rate determination (highlighted in green on Fig. DR4) is composed of packed, white limestone cobbles and large pebbles derived from limestone cliffs along the southern face of Büyük Dağ ("Big Mountain" in Turkish) 1.0-1.5 km north of the study site (Figs. DR2 and DR3). The surface of this fluvial terrace, which is quite planar, has been incised ~20 m by active streams that flow southward near the western and eastern edges of Ağılönü Canyon. These steep, high-energy mountain streams currently carry as bed load cobbles and large pebbles similar to those that make up the offset terrace. Figure DR5 shows our model for the sequential development of the mid-canyon terrace remnants (also shown as an inset in Fig. 2 of main text). Note that during right-lateral slip on the North Anatolian fault the southeastern corner of the terrace remnant north of the fault and the northwestern corner of the terrace remnant south of the fault will be exposed

to enhanced erosion by the modern, post-terrace streams. This model predicts that continued offset will yield rhomb-shaped terrace remnants that are very similar to those observed. The final drawing shows capture of the headwaters of the western stream by the eastern stream. This has occurred very recently at the study site, as shown by the extremely steep dip of the captured part of the stream system (see topographic map in Fig. 2 of main text).

Projection of the surface slope of the northern terrace fragment southward across the fault indicates 3.5±0.5 m of north-side-up separation. Relative to our offset measurement of 46±10 m, this yields a strike-slip: reverse slip ratio of ~13:1, indicating predominantly right-lateral strike-slip motion along the fault at Eksik, with a minor component of north-side-up contraction.

II. Discussions on offset measurement

There are two different offset features, of very different ages, present in Ağılönü Canyon; (1) a major bedrock canyon that has been offset ~200 m (Hubert-Ferrari et al., 2003); and (2) a much younger, ~46-m-offset of the inner edge of a late Holocene fluvial terrace (the focus of this study) that was deposited in a canyon incised into the base of the larger, older canyon.

The geomorphic evolution of the study site started with incision of the major bedrock canyon, inferred by Hubert-Ferrari et al. (2003) to have occurred ~10 ka in response to climatic changes at the end of the last glaciation. Following incision, this major canyon began to be offset by the NAF. Much later, probably during mid- or late Holocene time, a second downcutting event resulted in the development of a linear, incised valley inset into the base of the partially offset, older early Holocene canyon. This

second incision event was followed by an aggradational pulse that backfilled the younger inset canyon with fluvial gravels, forming a flat-topped, planar surface. It is this surface that we have dated in this study. Subsequent incision of this surface by the currently active drainages resulted in preservation of the fluvial terrace remnants described in this study. In light of the extremely steep stream gradient (>10º in the 60 m upstream of the fault, increasing gradually to >20º one km upstream) and resulting high-energy nature of these drainages, we think it likely that incision began soon after stabilization of the aggradational terrace surface. As discussed in the main text and below, the similar offsets of the buttress unconformity at the terrace inner edge and the incised, currently active drainages argue strongly for near-simultaneous terrace surface stabilization and subsequent incision.

The focus of this study is the younger, ~46 m offset of the late Holocene fluvial terrace. Specifically, we used the well-defined location of the inner edge of the terrace along the western edge of the canyon, in combination with the geometries of the currently active streams and the remaining terrace remnants, to determine the displacement along the North Anatolian fault at the Eksik site. The buttress unconformity at the terrace inner edge provides an easily recognized geomorphic feature that allows precise estimation of the offset. Moreover, because in most cases colluvial deposits cover the terrace inner edge at the Eksik site, it has been protected from post-terrace-abandonment erosion. In general, our mapping reveals that the terrace inner edge along the western margin of Ağılönü Canyon is relatively linear for several hundred meters both to the north and south of the fault, although the trend of the inner edge exhibits a gentle curve centered ~40 m north of the fault. Remnants of the terrace surface preserved along the edges of the

canyon and within the canyon are all at approximately the same elevation (relative to downstream position), indicating that the fluvial terrace was planar prior to incision by the current active streams.

In order to precisely determine the offset of the terrace inner edge, we created a detailed (50 cm contour interval) topographic map and surveyed all the major topographic and geologic features at the study site with a laser-range-finding theodolite with digital compass attachment. Specifically, we surveyed the limits of the preserved terrace surface remnants, the precisely determined positions of the buttress unconformity at the terrace inner edge revealed by both natural and trench exposures, the locations of incised, active drainages, the positions of all of our trenches and test-pits, and the locations of all geologic features that provide constraints on the location of the terrace gravels (e.g., bedrock exposures at the expected elevation of the terrace deposits, particularly the terrace surface).

On the detailed topographic map of our study site, shown in Fig. 2, the exact locations of the terrace inner edge are plotted as circles at locations where the buttress unconformity between the terrace deposits and the underlying bedrock-derived colluvium was exposed directly, either in natural, stream-cut exposures or our trenches. Other geomorphic and geologic features that provide limits on the location of the terrace inner edge, such as exposures of bedrock or bedrock-derived colluvium at the elevation of the terrace deposits, are shown with arrows pointing towards the contact.

Measurement of the western terrace inner edge

North of the fault (extending north from near the northwest corner of Fig. 2), the western inner edge of the terrace can be traced along a linear, south-flowing drainage that

has incised along the buttress unconformity between the underlying bedrock-derived colluvium and the upper surface of the onlapping terrace gravels. Bedrock and bedrock-derived colluvium are exposed at the elevation of the terrace surface to the west of the drainage. To the east of the drainage, however, a narrow, linear ridge composed of fluvial gravels locally preserves the planar terrace surface along its crest. The terrace inner edge lies between these two continuous exposures, within the ~10-m-deep incised drainage. This ~S20°E-trending, linear relationship can be traced northward for >200 m from the northernmost direct exposure of the terrace inner edge ~130 m north of the fault. Between the southern end of this linear drainage and the fault, the terrace inner edge is exposed in several natural, east-flowing side drainages, as well as within trench T2 (Figure 2). Trench TP2-06 is located 20 m north of the fault, about halfway between trench T2 and the fault. This 5-m-deep trench extended below the expected depth of the terrace surface at this location, as projected from the planar, mid-canyon terrace surface, yet exposed only bedrock-derived colluvium. If we have correctly projected the expected terrace elevation from the mid-terrace remnant to the site of trench TP2-06, this would indicate that the terrace inner edge lies to the east of trench TP2-06. In addition, we excavated trench TP1-06 at a lower elevation ~15 m to the east of TP2-06. Trench TP1-06 exposed a section of the basal contact between terrace fill deposits and underlying bedrock-derived colluvium. The base contact of the terrace gravels is ~2-3 m below the expected elevation of the terrace surface, indicating that the terrace inner edge lies to the west of trench TP1-06. Based on this constraint, and the exposure in trench T2, the trend of the inner edge must be more easterly than S34ºE, indicating that the inner edge exhibits a gentle downstream change in trend from S20ºE to ~S35-40ºE south of trench

T2, as it approaches the fault. Thus, the trend of the inner edge just north of the fault is similar to the linear, S40ºE trend of the inner edge south of the fault.

South of the fault, right-lateral offset of the east-facing, western side of Ağılönü Canyon has resulted in the development of a steep, ~15-m-high, south-facing fault scarp (as noted in the main text, true vertical uplift of the terrace surface is only ~3.5 m). Colluvium derived from this fault scarp has deeply buried the terrace inner edge immediately south of the fault, such that we could not expose it in our deepest trenches within ~35 m of the fault. The northernmost direct exposure of the terrace inner edge south of the fault is in trench T3, which is located ~2 m south of the break in slope at the base of the fault scarp (Fig. 2). The buttress unconformity at the terrace inner edge exposed in trench T3 trends S40°E. Forty meters south of T3, the terrace inner edge is exposed in two southeast-flowing drainages. Fifty meters south of these natural exposures, the inner edge is not covered by colluvium and can be mapped directly at the surface for several hundred meters downstream. Collectively, these exposures reveal a markedly linear, S40°E trend for the terrace inner edge south of the fault.

Although the area between the fault and trench T3 is covered by thick, fault-scarp-derived colluvium, a bedrock outcrop ~5 m south of the fault provides a constraint on the orientation of the terrace inner edge south of the fault. Specifically, the terrace inner edge just south of the fault cannot lie more than ~9 m west of the projection of the terrace inner edge based on its S40°E trend and location in and south of T3.

Taking all of these observations into consideration, we examined a range of potential offset reconstructions. As shown in Fig. 2 in the main text and in Fig. DR6, restoration of 46 m of right-lateral offset yields a geometrically simple alignment of the

western, terrace inner edge. The bedrock exposure 5 m south of the fault, together with

the projection of the terrace inner edge north of the fault, suggest a maximum-possible

offset of ~55 m. The minimum-possible offset of the inner edge is not tightly constrained

by available data.

In addition to our observations of the terrace inner edge, the incision associated

with the active eastern and western drainages, as well as the linear western edge of the

mid-canyon terrace remnant, provide additional, independent estimates of fault offset.

North of the fault, the western modern drainage has incised a 30-m-wide, S30ºE linear

canyon. Similarly, downstream of the ~50 m-wide zone of colluvial deposition off the

south-facing fault scarp, this drainage has cut a linear, S30ºE-trending canyon (Fig. 2).

The eastern modern drainage has incised a similar, S15ºW canyon north of the fault,

which gently curves downstream to a S20ºE trend south of the fault. Moreover, the

western edges of the terrace remnants both north and south of the fault exhibit similar,

linear S30ºE trends.

As shown in Figure 2 in the main text and in Fig.DR6, our preferred 46 m offset,

which is based on restoration of the western terrace inner edge, also restores the canyons

incised by the currently active drainages. Moreover, this preferred reconstruction also

approximately aligns the linear, S30ºE-trending western edges of the mid-canyon terrace

remnants. Figure DR6 illustrates restoration of these geomorphic features at five different

offsets ranging from 36 m to 56 m. This range is based on our preferred, 46 m offset,

together with symmetric epistemic ±10 m uncertainty. The maximum potential offset

(preferred 46±10 m) is based on a conservative amplification of the 55 m estimate of the

maximum possible offset described above. The minimum possible offset is not as well

constrained but, as shown in Fig.DR6 a suggested minimum offset of ~36 m (based on application of symmetric ±10 m error estimates) yields a geomorphically less likely reconstruction that does not properly align any of the major features discussed above.

III. Data From Fault-Parallel Trench

We excavated four fault-parallel trenches at the Eksik site to locate more accurately the terrace inner edges where they are not clearly exposed at the surface (Fig. DR7). The trenches were located as close as possible to the fault zone within the limitations of topography and thickness of overlying colluvium (see discussion below) (Fig. 2). Trenches T1, T2 and T3, which were excavated by hand and trenches TP1-06 and TP2-06, which were excavated by backhoe, were located on the western side of Ağılönü Canyon. Trench T4, which was excavated by backhoe, is located on the eastern terrace inner edge, north of the fault.

Trench T1, which was 6 m long and 50 cm wide, was excavated 22 m north of the fault on the western inner edge of the terrace. Trench T1 exposed bedrock at ~60 cm depth, indicating that the western inner edge of the terrace deposits is located to the east of the trench. This trench thus provides a limiting data point for the location of the western terrace inner edge north of the fault (shown by eastward-pointing arrow in Fig. 2).

Trench T2 was hand-excavated 10 m to the north of T1 and ~35 m north of the fault. The trench was 4.5 m long and 2.5 m deep. The western inner edge of the terrace gravels was exposed in three dimensions at 1.8 m depth, one meter from the western end of the trench (Fig. DR7). The terrace deposits are identical to those exposed elsewhere along Ağılönü Canyon, consisting of white- to pale-gray limestone cobbles and large

pebbles. The limestone clasts are angular-sub angular, consistent with relatively limited transport from the limestone cliffs 1.0-1.5 km upstream of the site. In trench T2, the terrace gravels are overlain along a planar contact by massive, dark-brown colluvium with bedrock pebbles in a silty clay matrix. Similar colluvium underlies the terrace gravels. The colluvium above the terrace gravels is overlain by coarser-grained, massive colluvium composed of abundant schist pebbles and angular to sub-angular schist boulders set in a silty sand matrix. The shallowest unit exposed in the trench is the 10- to 30-cm-thick weakly developed surface soil.

Trench T3 was hand-excavated parallel to, and 38 m south of the fault on the western inner edge. The trench was sited at the break in slope at the base of the prominent south-facing fault scarp. The trench was 10 m long and 2.5- to 2.8-m-deep. The surface soil is very thin (< 5 cm) and very weakly developed. The weak surface soil has developed down into dark brown, silty-sand colluvium that contains local bedrock clasts. As shown in Fig. 3, this massive colluvium overlies the terrace gravels along an irregular contact that contrasts markedly with the near-horizontal upper contacts of the terrace gravels observed in the other three trenches and in the exposures of the terrace deposits throughout Ağılönü Canyon. Specifically, the upper surface of the terrace gravels slopes sharply downward to the west, at a pronounced angle relative to near-horizontal layering within the gravels. We interpret these relationships as being indicative of erosion of the upper surface of the western-most part of the terrace gravels at the site of T3, probably during landsliding off the steep, south-facing fault scarp immediately north of the trench. The western-most exposure of the terrace gravels is located at meter 3 in the trench, at a depth of 2 m. In contrast, the terrace gravels extend as shallow as 0.5 m depth at the

eastern end of trench T3. In our reconstructions of the offset of the inner edge of the terrace gravels, we have used the actual western-most limit of the gravels at meter 3 in our minimum offset calculation, even though we strongly suspect that the original terrace inner edge was located farther west. By extrapolating the upper and lower contacts of the terrace gravels exposed in T3, we can estimate the approximate, pre-erosion location of the inner edge at ~meter 0 at the location of T3. We use this extrapolated location for our calculation of the preferred displacement of the western terrace inner edge.

Trench TP1-06 was excavated on the southwest-facing-slope along the western side of Ağılönü Canyon, parallel to and north of the fault. TP1-06, which was 10 m long and ~2 m deep, was excavated to provide an additional constraint on the terrace inner edge location between trench T2 and the fault. A section of the basal contact between terrace fill deposits (white limestone cobbles and small boulders) and the underlying bedrock-derived colluvium (dark gray colluvium containing highly altered, dark-green schist clasts) was exposed within TP1-06. The surface of this contact, however, is ~2 m below the expected elevation of the upper surface of the fluvial terrace gravels. Thus, data from TP1-06 indicates that the inner edge of the youngest terrace deposits is to the west of the trench.

Trench TP2-06 was excavated on the east side of Ağılönü Canyon, parallel to and 20 m north of the fault. TP2-06, which was 2 m long and ~5 m deep, exposed only highly altered, dark green bedrock and bedrock derived colluvium. The trench extended below the expected depth of the terrace surface at this location, as projected from mid-canyon, planar terrace surface. The absence of terrace gravels in TP2-06 thus indicate that edge of the youngest terrace deposits is located to the east of the trench.

Trench T4 was excavated on the eastern side of Ağılönü Canyon, parallel to and 8 m north of the fault. The trench was 12 m long and 2.5 m deep. In contrast to the exposures on the western side of Ağılönü Canyon described above, the ground surface on the east side of Ağılönü Canyon has been plowed during crop cultivation. The uppermost unit in this trench is a massive plow zone composed of silty-sandy dark brown soil containing bedrock clasts. The terrace deposit consists of a relatively thin gravel sheet that pinches out eastward at m1.5 and thickens westward from ~20 cm at meter 2 to 40-55 cm at the west end of the trench (m 12). The top of the terrace deposit is relatively planar and nearly horizontal. The terrace gravels are similar to those exposed elsewhere at the site, consisting of angular to sub angular, pale gray-white limestone cobbles and large pebbles. The youngest terrace gravel unit is underlain by bedrock-derived colluvium with a silty-sandy clay matrix. A thin (~10 cm thick) yellowish-brown, silty clay lens within this unit that extends from meter 3 to 10. An older gravel unit is exposed from meter 10.8 to the western end of the trench. In marked contrast to the terrace gravels, this unit includes both limestone and bedrock-derived clasts. We interpret this deeper gravel as an older phase of fluvial deposition in which colluvium derived from bedrock slopes ~70 m to the north of the trench was mixed with river-borne limestone gravels prior to deposition at the trench site.

IV. ^{36}Cl Surface Exposure Dating Results

The ^{36}Cl ages for the ten limestone cobbles collected from the surface of the offset fluvial terrace were calculated using the program CHLOE (CHLOrine-36 Exposure age) (Phillips and Plummer, 1996)(Fig. DR7, Tables DR1 and DR2). This version of CHLOE employed the thermal and epithermal neutron distribution equations of (Phillips et al.,

2001) and production of [36]Cl by muons according to (Stone et al., 1998). The [36]Cl production parameters of (Phillips et al., 1996) were used, as corrected by (Phillips et al., 2001) for the new neutron distribution equations and the incorporation of production from muons. Production rates of [36]Cl from Ca and K were determined by principal factor analysis of whole rock data (Phillips et al., 1996) and by measurement of mineral separates (Stone et al., 1996) and (Evans et al., 1997). The values of the three critical production parameters were 66.8 atoms [36]Cl (g Ca)[-1] yr^{-1}, 154 atoms [36]Cl (g K)[-1] yr^{-1}, and 626 epithermal neutrons (g air)[-1] yr^{-1}, based on Phillips et al. (1996). We also calculated the ages of the [36]Cl samples using the production rates of Stone et al. (1996) for Ca , (48.4 atoms 36ck (g Ca)[-1] yr^{-1}), and Evans et al. (1997) for K, (170 atoms [36]Cl (g K)[-1] yr^{-1} (Table DR4). Snow shielding, shielding by surrounding topography, and effects of non-horizontal surfaces were negligible and no correction was made for these parameters. All analytical uncertainties are reported as plus-or-minus one standard deviation and incorporate only the reported AMS analytical uncertainty in the [36]Cl measurement. Consideration of all sources of uncertainty would probably result in 10% to 15% standard deviations (Phillips et al., 1996). A more complete description of the dating methodology and shielding calculations can be found in Gosse and Philips (2001). The relevant exposure conditions and chemical compositions of the samples are shown in Table DR1 and DR2, respectively.

V. Radiocarbon Ages

A total of eight charcoal samples were radiocarbon dated to independently constrain the age of the offset Eksik terrace deposits (Table DR3 and 4). Five of these samples were collected from trench T4 along the east side of Ağılönü Canyon, two were

collected from trench T2, and one was collected from T-3, both along the west side of the canyon. All samples were dated at the Center for Accelerator Mass Spectrometry (CAMS) at Lawrence Livermore National Lab. All samples were calibrated using the program OxCAL (Bronk Ramsey, 1995; 2001, using atmospheric data from Reimer et al., 2004). OxCAL is available online at: http://c14.arch.ox.ac.uk/oxcal.php.

As discussed in the main text, we recovered three samples (EX-4-1, EX-4-3, and EX-4-4) from beneath the youngest terrace gravels. As can be seen from the trench log of trench T4 (Fig. DR8), these samples were collected from beneath the thin sheet of limestone cobbles and pebbles that represent the youngest phase of fluvial gravel deposition, and hence the age of initial stabilization of the terrace surface, along the eastern edge of Ağılönü Canyon. The radiocarbon ages for these samples were in correct stratigraphic order, with the shallowest samples (EX-4-1 and EX-4-4) yielding overlapping, calibrated dates of 2.81-2.92 ka and 2.42-2.92 ka, respectively (Fig. DR7 and 8). Sample EX-4-3, collected 95 cm beneath EX-4-4, yielded a slightly older calibrated age of 2.92-3.22 ka. In addition to these three dates from beneath the shallowest terrace gravels, we also recovered charcoal samples from within, and just above, the terrace deposits. The only radiocarbon sample recovered from within the terrace gravels (EX-4-2) yielded an anomalously old, calibrated calendric age of 3.50-4.05 ka, reflecting reworking. However, a charcoal sample recovered from 20 cm above the top of the shallowest terrace gravels in trench T4 (EX-4-5) yielded a calibrated age of 2.06-2.12 ka. The consistency of these radiocarbon dates (with the exception of sample EX-4-2 from within the gravels) indicates minimal reworking, suggesting that these samples may provide a reliable estimate of the age of the colluvial deposits that

immediately over-and underlie the youngest, shallowest part of the terrace gravels. These radiocarbon age data thus provide an independent constraint on the age of the terrace surface and on the general validity of the ^{36}Cl production rates used in the cosmogenic age calculations discussed in the main text.

In addition to the five samples dated from trench T4, we also collected two samples from trench T2. Both were collected from near the western inner edge of the terrace. Sample EX-2-2 was collected from colluvium 10 cm below the base of the terrace gavels, whereas EX-2-1 was collected from colluvium 20 cm above the top of the gravels, at a depth of 1.4 m (Fig. DR8). Both of these samples yielded much older ages than the ^{14}C samples recovered from T4, suggesting that the T2 samples are reworked from older deposits. Specifically, sample EX-2 –2 yielded a calibrated age of 5.00-5.48 ka, and sample EX-2-1 yielded a calibrated age of 4.53-4.93 ka. We also recovered one sample from trench T3. Sample EX-3-1 was collected at 85 cm depth, from colluvium just above the terrace gravels (Fig. DR5). However, as discussed above, we suspect that the interval from which EX-3-1 was recovered is part of a shallow landslide that has disturbed the top of the terrace gravels at this location. Thus, we do not have confidence that the 2.06-2.47 ka age of this sample provides a precise constraint on the age of the terrace gravels, although it is generally consistent with both the ^{14}C sample ages from trench T4 and with the cosmogenic surface exposure ages from the terrace deposit.

Data Repository References

Barka, A. A., 1996, Slip distribution along the North Anatolian fault associated with large earthquakes of the period 1939-1967: Bulletin of the Seismological Society of America, v. 86, no. 5, p. 1238-1254.

Bronk Ramsey, C., 1995, Radiocarbon Calibration and Analysis of Stratigraphy: The OxCal Program: Radiocarbon, v. 37(2), p. 425-430.

Bronk Ramsey, C., 2001, Development of the Radiocarbon Program OxCal: Radiocarbon, v. 43 (2A), p. 355-363.

Evans, J. M., J. O. H. Stone, L. K. Fifield and R. G. Creswell, 1997, Cosmogenic chlorine-36 production in K-feldspar. Nuclear Instruments and Methods in Physics Research 123: 334-340.

Gosse J. C. and Phillips F. M., 2001, Terrestrial in-situ cosmogenic nuclides: Theory and application: Quaternary Science Reviews 20 1475-1560.

McClusky, S, Balassanian, S., Barka, A., Demir, C., Ergintav, S., Georgiev, I, Gurkan, O., Hamburger, M., Hurst, K., Kahle, H., Kastens, K., Kekelidze, G., King, R., Kotzev, V., Lenk, O., Mahmoud, S., Mishin, A., Nadariya, M., Ouzounis, A., Paradissis, D., Peter, Y., Prilepin, M., Reilinger, R., Sanli, I., Seeger, H., Tealeb, A., Toksöz, M. N., and Veis, G., 2000, Global positioning system constraints on plate kinematics and dynamics in the eastern Mediterranean and Caucasus: Journal of Geophysical Research, v. 105, no. 3, p. 5695-5719.

Phillips F. M. and Plummer M. A., 1996, CHLOE: A program for interpreting in-situ cosmogenic nuclide data for surface exposure dating and erosion studies: Radiocarbon (Abstr. 7th Int. Conf. Accel. Mass Spectrom.) 38 98-99.

Phillips F. M., Zreda M. G., Flinsch M. R., Elmore D., and Sharma P., 1996, A reevaluation of cosmogenic ^{36}Cl production rates in terrestrial rocks: Geophysical Research Letters 23 949-952.
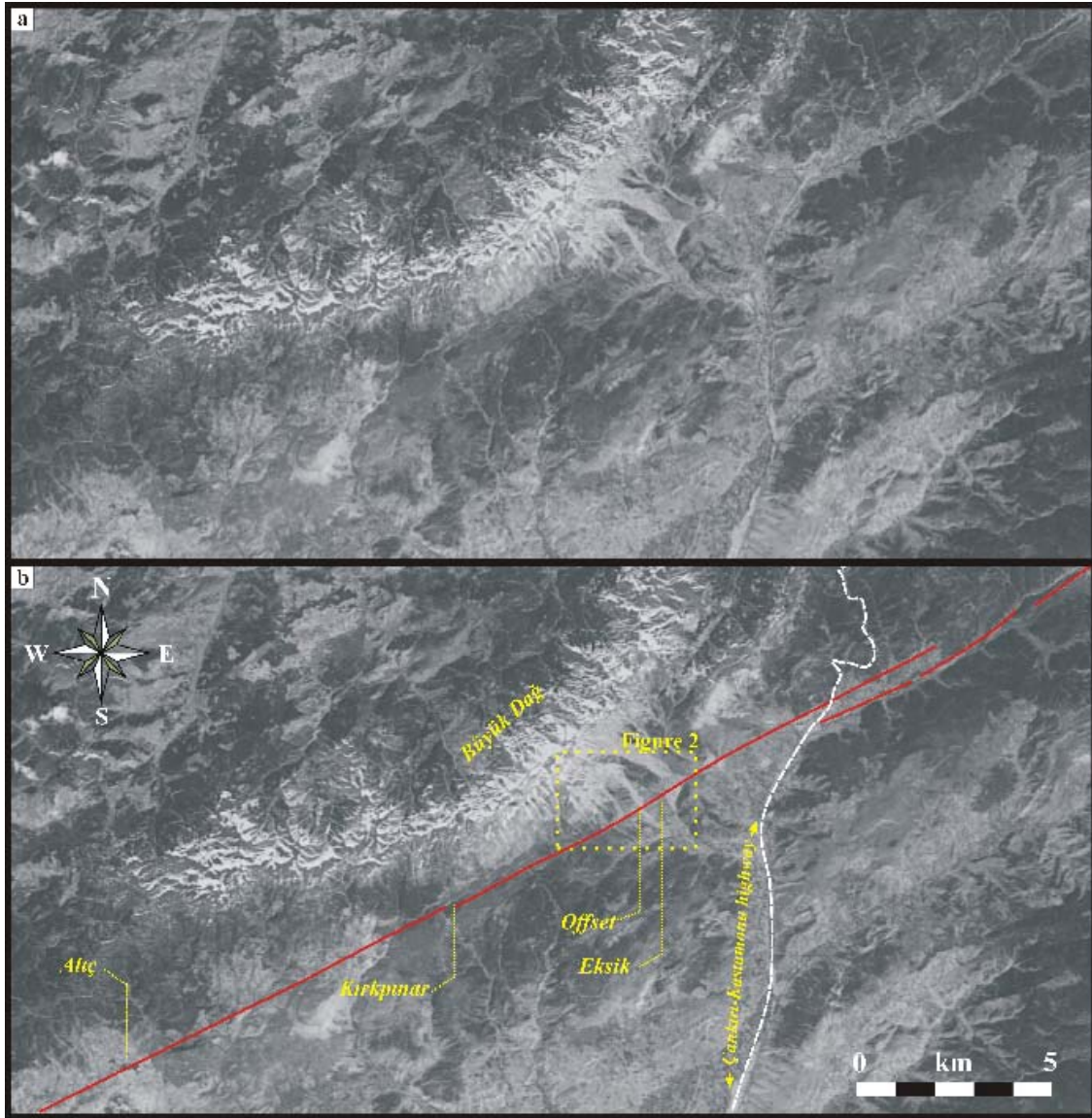
Phillips F. M., Stone W. D., and Fabryka-Martin J. T., 2001, An improved approach to calculating low-energy cosmic-ray neutron fluxes near the land/atmosphere interface: Chemical Geology 175 689-701.

Reimer P.J., Baillie, M.G.L., Bard, E., Bayliss, A., Beck, J.W., Bertrand, C., Blackwell, P.G., Buck, C.E., Burr, G., Cutler, K.B., Damon, P.E., Edwards, R.L., Fairbanks, R.G., Friedrich, M., Guilderson, T.P., Hughen, K.A., Kromer, B., McCormac, F.G., Manning, S., Bronk Ramsey, C., Reimer, R.W., Remmele, S., Southon, J.R., Stuiver, M., Talamo, S., Taylor, F.W., van der Plicht, J., and Weyhenmeyer, C.E., 2004, Radiocarbon Calibration from 0-26 cal kyr BP - IntCal04 Terrestrial Radiocarbon Age Calibration, 0-26 cal kyr BP: Radiocarbon, v. 46, p. 1029-1058.

Stone, J. O., G. L. Allan, L. K. Fiefield and R. G. Cresswell, 1996, Cosmogenic chlorine-36 from calcium spallation. Geochimica et Cosmochimica Acta 60(4): 679-692.

Stone J. O. H., Evans J. M., Fifield L. K., Allan G. L., and Cresswell R. G., 1998, Cosmogenic chlorine-36 production in calcite by muons: Geochimica et Cosmochimica Acta 62 433-454.

Sugai, T., Emre, Ö., Duman, T., Kuşçu, İ., and Yoshioka, T., 1998, SGJ-MTA Int'l Coop. research on the Anatolian Paleoseismicity, Interim report on active fault and paleoearthquake research in 1998: Geological Survey of Japan Interim Report EQ/99/3, p. 263-273.
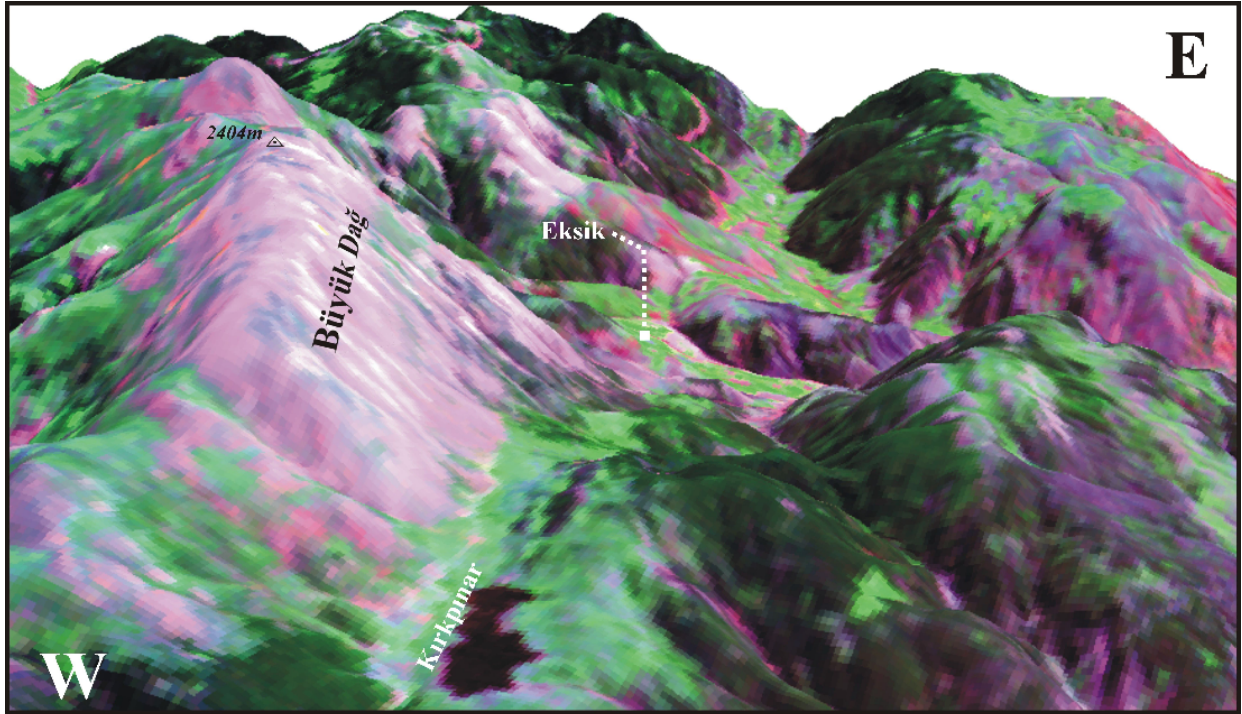
DATA REPOSITORY FIGURES

Kozaci et al., Figure DR-1

Figure DR1 Regional tectonic map showing major active structures (modified from Barka, 1996). Eksik study site along the central North Anatolian fault denoted by white circle. Large arrows show GPS rates generalized from McClusky et al. (2000). Background satellite image provided by NASA Earth Observatory. DSF=Dead Sea fault; EAF=East Anatolian fault.
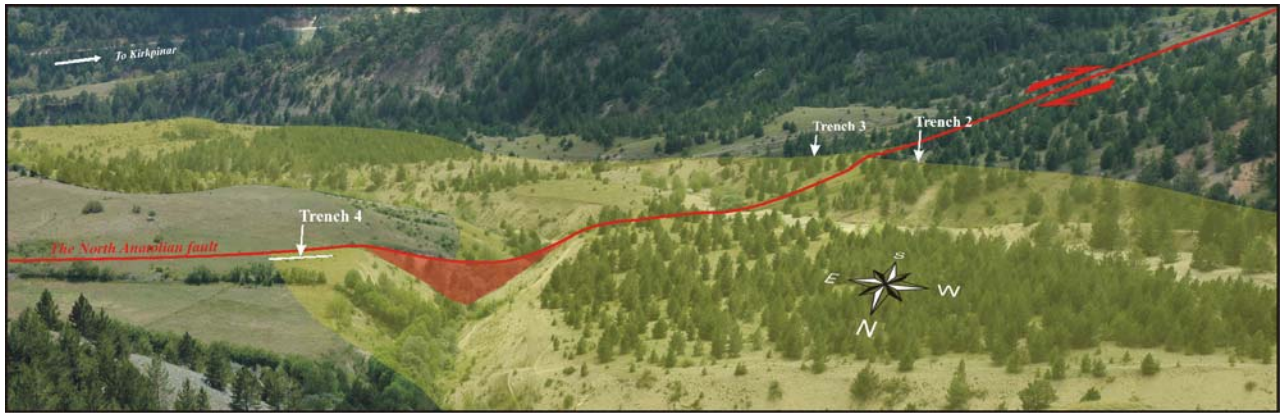
Figure DR2 Corona satellite image showing the region surrounding the Eksik study site. (a) Uninterpreted Corona image. (b) Corona image showing the trace of the North Anatolian fault, and part of the Cankiri-Kastamonu highway. Note location of Alıç paleoseismologic study site of Sugai et al., (1998).
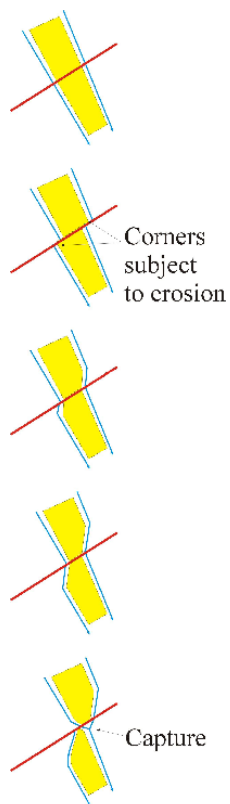
Kozaci et al., Figure DR-3

Figure DR3 Three-dimensional virtual view of the North Anatolian fault in the region near Eksik looking ENE. The image was created by draping a Landsat image over 90 m DEM (Digital Elevation Model). No vertical exaggeration. Büyük Dağ ("Big Mountain") is the source of the limestone gravels that form the fluvial terrace discussed in this paper.

Figure DR4 A panoramic view of the Eksik slip rate site looking south-southwest across

the North Anatolian fault (NAF) (red) and dissected and offset fluvial terrace discussed in

the paper. The bright green overlay shows the extent of the fluvial terrace deposits.

Kozaci et al., Figure DR-5 jpeg

Figure DR5 A simple model suggesting the sequential evolution of the geometry of the terrace during recurrent displacements along the North Anatolian fault. Note the similarity between the final stage of the model and the mapped mid-canyon terrace remnants.

Kozaci et al., Figure DR-6 jpeg

Figure DR6 Offset reconstructions of four geomorphic features; (1) western inner edge of the youngest terrace deposits, (2) and (4) the active flood plain, and (3) the edges of the flat-topped mid-canyon terrace remnant with 5 m increments. Please note that the 46 m preferred offset reconstruction is based on the precisely determined positions of the buttress unconformity at the terrace inner edge west of the canyon (1).
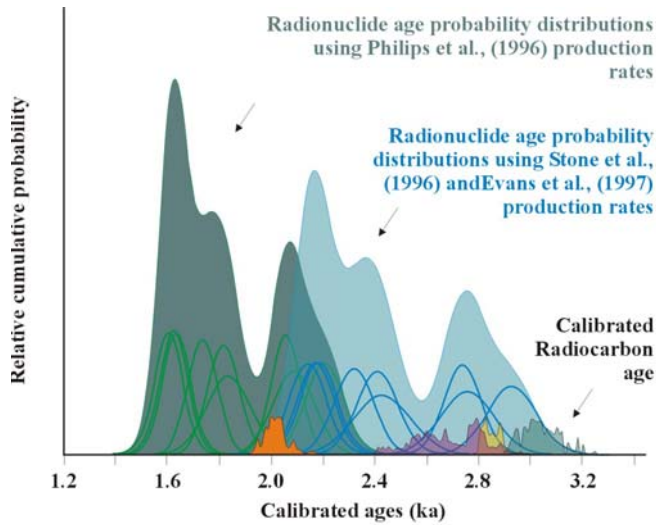
DR2007218

Figure DR7 Plot of [^36]Cl surface exposure ages and [^14]C charcoal ages for samples collected from beneath ([^14]C-1, 3 and 4) and above ([^14]C-5) the terrace gravels in the Trench T4. Simple Gaussian probability distribution functions (pdfs) for ^{36}Cl data created in Matlab using Camelplot (Balco, personal communication). Radiocarbon pdfs data created in OxCAL (Bronk Ramsey, 1995; 2001; using atmospheric data from Reimer et al., 2004). For the ^{36}Cl ages the green and blue lines are Gaussian probability distributions for the individual ^{36}Cl measurements. Probability values are normalized so that each individual probability distribution has unit area. Shaded areas are sum of probability distributions for all samples. For ^{14}C the plots give calibrated probability distributions from OxCal normalized to unit probability. The ordinate axis gives relative values independently for ^{36}Cl and ^{14}C.
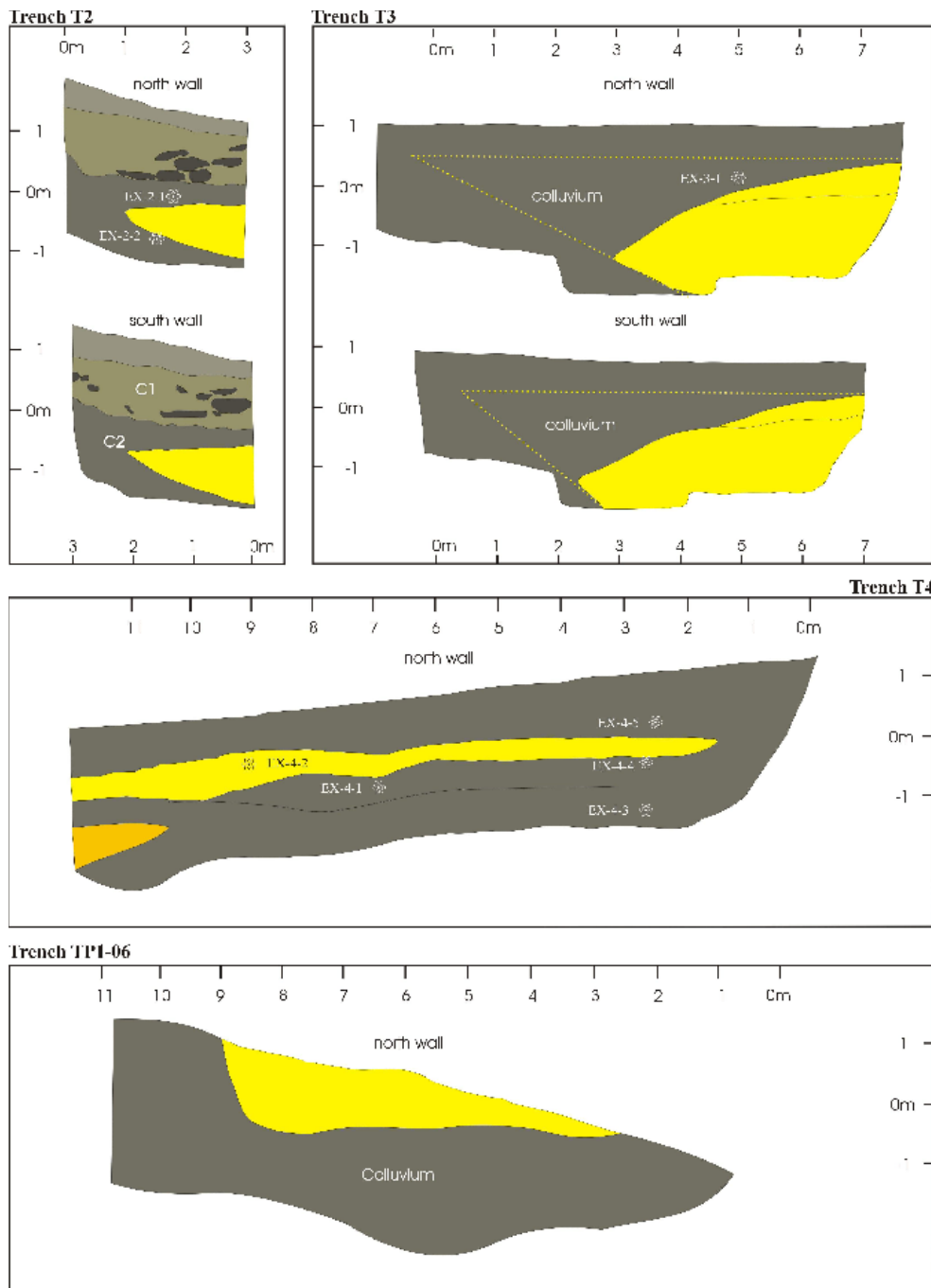
Figure DR8 Logs of trenches T2, T3, T4 and TP2-06. Terrace gravels are shown in yellow and yellow-orange. Olive green denotes bedrock-derived colluvium. C1 and C2 represent different bedrock-derived colluvium units within T-2 based on change in clast size. Dashed lines on logs of trench T-3 show the probable original extent of the terrace

inner edge. This interpretation is based on the unusual west-dipping upper surface of the terrace deposits and trucation of sub-horizontal layering within the terrace gravels, which suggest that the upper contact of the terrace gravels has been disturbed, probably by shallow landsliding. Although the extrapolated terrace inner edge location at m 0 is used for our preferred offset measurement, the actual measured minimum exposed extent of the inner edge (i. e. m 2.5) is used for the calculation of the minimum offset discussed in the text. Trench T1 and TP2-06 exposed only dark-grayish-green bedrock-derived colluvium and schist bedrock Therefore, the logs for these trenches are not shown.
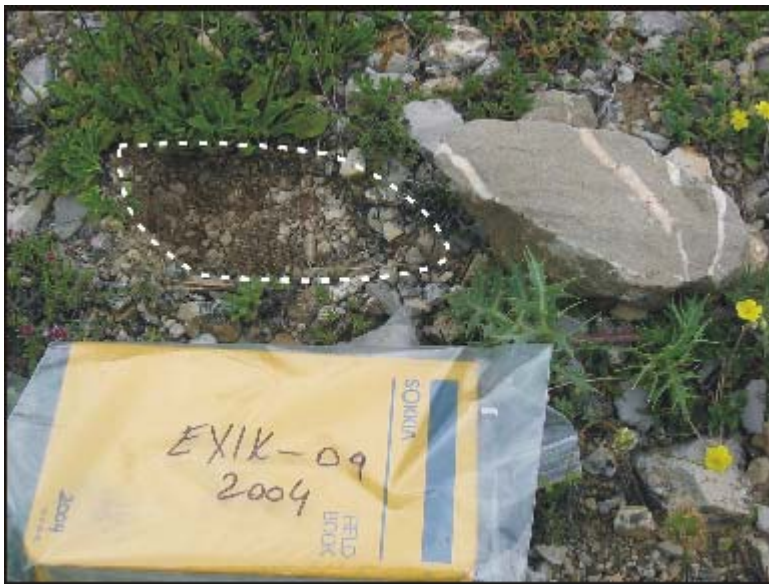

Figure DR9 An example of the sampled limestone cobbles collected for surface exposure dating. The samples were collected where they were embedded in a pavement composed of small pebbles and soil. They have smoother and soil-stained lower surfaces indicating little or no movement during their exposure history. Dashed line shows location of the sample before it was collected.

Table DR1 Location and size of ^{36}Cl surface samples from Eksik study site.

Eksik, Turkey Surface Samples (^{36}Cl)

Sample #	Lab ID	Latitude (N)* (d m.mmm)	Longitude (E)* (d m.mmm)	Elev (m)'	Rock Type	Thickenss (cm) (cm)
^{36}Cl-1	TE-S-10	41 01.158	33 40.199	1453	Limestone	5
^{36}Cl-2	TE-S-9	41 01.134	33 40.206	1449	Limestone	5
^{36}Cl-3	TE-S-8	41 01.120	33 40.211	1442	Limestone	4
^{36}Cl-4	TE-S-7	41 01.112	33 40.209	1440	Limestone	5
^{36}Cl-5	TE-S-6	41 01.073	33 40.204	1426	Limestone	5
^{36}Cl-6	TE-S-5	41 01.062	33 40.206	1426	Limestone	5
^{36}Cl-7	TE-S-1	41 01.062	33 40.208	1427	Limestone	5
^{36}Cl-8	TE-S-2	41 01.056	33 40.210	1426	Limestone/Marble	6
^{36}Cl-9	TE-S-3	41 01.052	33 40.214	1424	Limestone	5
^{36}Cl-10	TE-S-4	41 01.040	33 40.226	1420	Limestone	4

Table DR2 Chemical compositions of ^{36}Cl samples. Note that major elements are in weight percent. Trace elements are in parts per million. LOI is loss on ignition. Fe$_2$O$_3$-T is total iron expressed as Fe$_2$O$_3$. ND is below the lower limit of determination.

EKSIK, TURKEY ^{36}Cl Surface Samples - Chemical Compositions

Sample	Sample Wt	Carrier Wt	Carrier Conc	^{36}Cl/^{37}Cl	Cl/Cl (at/at in rock)	Cl (ppm)	SiO$_2$	TiO$_2$	Al$_2$O$_3$	Fe$_2$O$_3$-T	MnO	MgO	CaO	Na$_2$O	K$_2$O	P$_2$O$_5$	LOI	Total	Ba	Rb	Sr
	g	g	mg/g	(10^{-15})	at/at in rock	ppm	%	%	%	%	%	%	%	%	%	%	%	%	ppm	ppm	ppm
TE-S-1	150.06	3.023	0.993	94	165	20.3	21.55	0.02	0.81	0.53	0.07	0.65	40.61	0.12	0.08	0.03	35.46	100.13	66	ND	2865
TE-S-2	111.40	2.992	0.993	99	218	18.8	45.41	0.02	0.86	0.55	0.06	0.44	27.67	0.14	0.08	0.02	24.06	100.25	63	ND	2335
TE-S-3	150.67	3.014	0.993	148	191	38.5	11.87	0.02	0.71	0.16	ND	0.74	47.64	0.06	0.04	0.02	39.27	100.53	65	ND	2511
TE-S-4	150.50	3.002	0.993	201	325	23.8	5.58	0.02	1.33	0.08	0.01	0.59	49.31	0.06	0.05	0.02	41.78	98.63	ND	ND	2424
TE-S-5	146.50	3.001	0.993	175	230	37.6	3.04	0.02	0.97	0.64	0.12	0.66	50.44	0.14	0.05	0.02	41.91	99.33	ND	ND	3760
TE-S-6	96.65	3.035	0.993	168	301	31.0	14.32	0.04	1.25	0.26	0.01	0.71	44.67	0.08	0.17	0.05	38.32	100.06	60	6	2542
TE-S-7	150.50	3.029	0.993	179	250	32.3	4.86	0.02	0.14	0.11	ND	0.72	51.63	0.06	0.04	0.02	42.23	99.83	ND	ND	2873
TE-S-8	150.18	3.018	0.993	203	266	37.5	3.79	0.02	1.09	0.2	ND	0.65	50.5	0.06	0.04	0.02	42.46	99.05	76	ND	2812
TE-S-9	150.40	3.023	0.993	170	209	43.6	2.54	0.02	0.69	0.96	0.11	1.11	52.19	0.14	0.04	0.03	42.35	100.18	44	ND	2316
TE-S-10	150.30	3.030	0.993	222	317	30.8	3.44	0.01	0.59	0.09	ND	1.16	51.01	0.06	0.05	0.04	42.85	99.1	ND	ND	2511

Table DR3 Radiocarbon ages from fault parallel trenches at the study site.

Eksik, TURKEY, [14]C Samples									
CAMS #	Sample Name	Sample Location	$\delta^{13}C$	fraction Modern	±	$D^{14}C$	±	[14]C age	±
118239	EX-4-1	Trench T4	-25	0.7149	0.0027	-285.1	2.7	2695	35
120517	EX-4-2	Trench T4	-25	0.6503	0.0054	-349.7	5.4	3460	70
118240	EX-4-3	Trench T4	-24.5	0.6999	0.0038	-300.1	3.8	2865	45
120518	EX-4-4	Trench T4	-25	0.7244	0.0066	-275.6	6.6	2590	80
118241	EX-4-5	Trench T4	-24.8	0.7776	0.0025	-222.4	2.5	2020	30
118242	EX-2-1	Trench T2	-24.2	0.6022	0.0020	-397.8	2.0	4075	30
118243	EX-2-2	Trench T2	-22.2	0.5718	0.0019	-428.2	1.9	4490	30
118244	EX-3-1	Trench T3	-25.0	0.7613	0.0026	-238.7	2.6	2190	30

Table DR4 Summary of slip rate calculations including estimates using all nine [36]Cl samples as well as preferred sub-cluster of six youngest [36]Cl ages for production rate of Stone et al., (1996) and Evans et al., (1997), and Philips et al., (1996). Rates based on radiocarbon ages are shown both for minimum rate based solely on age range of youngest charcoal fragment recovered from beneath the shallowest terrace gravels, and for the full slip rate based on over-and underlying samples.

Slip Rate Calculation Summary Table					
	Stone et al., (1996) and Evans et al., (1997) [36]Cl production rates		Philips et al., (1996) [36]Cl production rates		[14]C
	age range for 9 samples	age range for 6 samples	age range for 9 samples	age range for 6 samples	min	preferred
age (ka)	2.14-2.93	2.14-2.43	1.61-2.21	1.61-1.84	<2.42-2.92	1.95-2.92
offset (m)	46±10	46	46±10	46±10	46±10	46±10
slip rate (mm/yr)	12-26 (19±7)	15-26 (20.5±5.5)	16-35 (25.5±9.5)	20-35 (27.5±7.5)	>12-23 (17.5±5.5)	12-28 (20.5±8.5)